Approaching C1 Reaction Mechanisms Using Combined *Operando* and Transient Analysis: A Case Study on Cu/CeO_2 Catalysts During LT-Water–Gas Shift Reaction

Marc Ziemba, Jakob Weyel, Christian Hess*

Eduard Zintl Institute of Inorganic and Physical Chemistry, Technical University of Darmstadt, Alarich-Weiss-Str. 8, 64287 Darmstadt, Germany

*email: christian.hess@tu-darmstadt.de

Keywords

Mechanism, Cu/CeO_2, water–gas shift, *operando* spectroscopy, transient spectroscopy, Raman, DRIFTS, UV-Vis

TOC Graphic

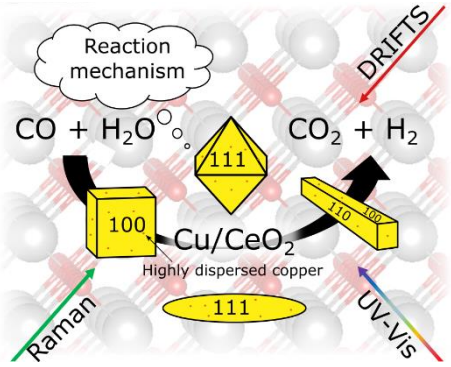
Reaction mechanism
DRIFTS
CO + H2O
CO2 + H2
111
100
110
100
Cu/CeO2
Highly dispersed copper
111
Raman
UV-Vis

Abstract

The elucidation of reaction mechanisms is an essential part of catalysis research, providing approaches to improving catalysts or, ultimately, to designing catalysts based on a profound understanding of their mode of operation. In the context of C1 processes, redox or/and associative mechanisms have been proposed in the literature but their critical assessment has been a major challenge. Here, we highlight the importance of applying a combination of techniques suited to addressing both the redox properties and intermediate/adsorbate dynamics in a targeted manner. We illustrate our approach by exploring the mechanism of LT-WGS over low-loaded Cu/CeO_2 catalysts, using different ceria morphologies (sheets, polyhedra, cubes, rods) to study the influence of the surface termination. While the results from *operando* Raman and UV-Vis spectroscopy are consistent with a redox mechanism, there is no direct correlation of activity with reducibility. Probing the subsurface/bulk oxygen dynamics using *operando* Raman F_{2g} analysis coupled with $H_2{}^{18}O$ highlights the importance of transport properties and the availability of oxygen at the surface. Transient IR spectra reveal the presence of different surface carbonates, none of which are directly involved in the reaction but rather act as spectator species, blocking active sites, as supported by the facet-dependent analysis. From transient IR spectroscopy there is no indication of the involvement of copper, suggesting that the catalytic effect of copper is mainly based on electronic effects. The results from the *operando* and transient analysis unequivocally support a redox mechanism for LT-WGS over Cu/CeO_2 catalysts and demonstrate the potential of our combined spectroscopic approach to distinguish between redox and associative mechanisms in oxide-supported metal catalysts.

1. Introduction

Hydrogen plays a central role in the production of fine chemicals and in the energy sector. As its main source is the reforming of hydrocarbons,[1] it will be essential to use alternative sources, such as water splitting and the conversion of water in the framework of the water–gas shift (WGS) reaction, in the future. In addition, the WGS reaction plays an important role in adjusting the amount of hydrogen and carbon monoxide for fuel cell applications.[2] It is therefore of great importance to find efficient and cost-effective WGS catalysts that run efficiently even at low temperatures (<200 °C). Metal-loaded ceria has been proven to be a good alternative to the conventional copper–zinc oxide catalysts used in industry,[3–6] but important aspects such as the reaction mechanism, the role of the metal, and the influence of the ceria support properties are still a matter of debate.

In the context of the WGS reaction, but also C1 processes (e.g. reverse WGS, RWGS), redox or/and associative mechanisms have been proposed in the literature. In the redox mechanism, adsorbed CO is oxidized to CO_2 by lattice oxygen from the support, leading to oxygen vacancy formation. The latter is replenished by water after O-H bond cleavage, while hydrogen atoms combine to H_2. Associative mechanisms are based on the formation of surface intermediate species, starting from adsorbed CO and support hydroxyl groups, and their decomposition to CO_2 and hydrogen. As intermediates, formate,[7–9] carbonate[10,11], carboxyl / carboxylate[12–15] and hydroxycarbonyl[16] species have been proposed. In earlier work on ceria-supported noble metals (Pt, Pd, Rh, Au), a redox mechanism was proposed,[17,18] while later, by use of IR spectroscopy, an associative formate-based mechanism was suggested[19] and critically discussed.[20] Based on steady-state isotopic transient kinetic analysis on Pt catalysts, formate was excluded from being an important intermediate.[8] Water dissociation was reported to be energetically important for the WGS reaction,[8,13,21–24] but not rate-limiting, as shown for Pt[14] and Au[25] catalysts. Regarding Cu/CeO_2 catalysts, in particular the interaction of metallic copper with oxygen vacancies (O_{vac}) was reported to enhance the reactivity,[26] as supported by studies on the inverse CeO_2/CuO-Cu system, where defect-rich ceria was proposed to be mainly responsible for water dissociation and metallic copper for providing adsorbed CO for the reaction.[27] In later studies, carbonates were proposed as intermediates using *operando* SSITKA-DRIFTS[28] (steady-state isotropic transient kinetic analysis–diffuse reflectance Fourier transform spectroscopy) and *in situ* DRIFTS,[29] but in the latter study stationary measurements in helium as background were performed, therefore not allowing a definite statement on the mechanism. Thus, in the literature, two main mechanisms are currently being discussed for

supported metal oxide catalysts, namely the redox and associative mechanisms, and which mechanism is ultimately the more important and dominant one is not yet fully resolved.[30,31]

Cu/CeO_2 catalysts have recently received increasing attention, showing good conversions in low-temperature (LT-)WGS.[29,32–34] According to literature reports, the catalytic activity increases with the Cu loading;[35,36] therefore, most studies have focused on highly loaded catalysts.[29,33,37] However, normalized to the Cu content, the low-loaded catalysts show higher conversions.[36] Nevertheless, there are no detailed mechanistic studies on the loading dependence of the mechanism itself. In addition, it is worth mentioning that the method of loading copper onto the support has great influence on the catalytic activity, as it can affect the copper dispersion and particle size.[34,37] For example, it has been shown that mesoporous copper-cerium-titania composites prepared by chemisorption-hydrolysis exhibit a higher activity than those prepared by incipient wetness impregnation due to the presence of finely dispersed CuO particles.[38] In this context is it worth mentioning that our previous studies on Au/CeO_2 catalysts, exhibiting highly dispersed Au particles, have demonstrated facet-dependent agglomeration of gold during reaction, limiting the WGS activity.[39,40]

Previous literature studies on Cu/CeO_2 catalysts have highlighted the importance of the copper oxidation state,[26,34,36,41] which depends on both the gas-phase environment and the loading.[36,42,43] On one hand, the interaction of metallic copper with oxygen vacancies (O_{vac}) was reported to enhance the reactivity,[26] while on the other, copper was shown to have an oxidation state of +1 at the interface and to participate in the reaction,[44] as supported by other studies, demonstrating the stability of oxidized copper under reductive conditions.[45] In addition, a strong dependence of the state of copper on the gas phase at 180 °C was observed for 20 wt% Cu/CeO_2, i.e., mainly Cu^0 was detected during CO exposure and Cu^+ in the subsequent exposure to an inert gas.[42] At low loadings, e.g. 1 wt% Cu/CeO_2, the catalyst behaves differently, as rather Cu^+ is observed under CO atmosphere, which is then further oxidized to Cu^{2+} on switching to He,[43] indicative of electronic metal–support interactions.

Another important parameter for the Cu–ceria interaction and the reactivity behavior is the selection of the ceria facet. To this end, theoretical studies have revealed a dependence on the strength of the interaction of Cu with the low-index surface facets,[34,46] which is also reflected in the catalytic activity.[29,32–34,47] For 5 wt% Cu/CeO_2 catalysts, octahedra were found to exhibit the highest WGS activity at ≥200 °C, followed by rods and cubes, by providing the best Cu dispersion, the largest amount of moderately active copper oxide, and the strongest Cu–support interaction.[29] To summarize previous literature findings, the state of copper when supported by ceria strongly depends on the copper loading, and so far a major focus has been

placed on highly loaded catalysts. Thus, various aspects, such as the dependence of the mechanism on copper loading, oxygen/defect dynamics during reaction, and the role of copper and its state, are not sufficiently clarified.

In this study, we address the WGS reaction mechanism of low-loaded Cu/CeO_2 catalysts. To this end, it is important to develop approaches that enable the redox properties to be monitored on the one hand and the surface intermediate dynamics on the other. Thus, we combined *operando* Raman and UV-Vis spectroscopy as well as isotopic labeling by $H_2{}^{18}O$ to probe (sub)surface properties. Modulation excitation (ME-)DRIFTS measurements with its increased sensitivity towards adsorbates,[48] complemented by quasi *in situ* XPS, allowed us to study the support and (transient) adsorbate dynamics as well as the surface state of Cu/CeO_2 catalysts in an integrated manner. Besides the mechanistic aspects, we address the role of ceria surface facets, highlighting the importance of the support properties, and compare our findings with those obtained previously for Au/CeO_2 catalysts,[25,39,40] underlining the role of the supported metal.

2. Experimental Section

2.1 Catalyst Preparation

Polycrystalline ceria sheets were prepared by thermal decomposition of $Ce(NO_3)_3 \cdot 6H_2O$ (Alfa Aesar, 99.5 %) at 600 °C as described in our previous studies.[49,50] Ceria cubes and rods were prepared by hydrothermal synthesis of $CeCl_3 \cdot 7H_2O$ (Alfa Aesar, 99%) and $Ce(NO_3)_3 \cdot 6H_2O$ (Alfa Aesar, 99.5%) in a NaOH solution (98%, Grüssing GmbH) as described in our previous studies.[39,51] Ceria polyhedra or octahedra were purchased from Sigma Aldrich (<25 nm (BET)).

Copper was loaded onto ceria via deposition-precipitation (DP) using a 10^{-3} M $CuCl_2 \cdot 2H_2O$ solution (Sigma Aldrich, ≥99.5 %), by first redispersing the ceria samples in a ratio of 1:150 in deionized water and adjusting the pH to 9 using a 0.1 M NaOH solution (98%, Grüssing GmbH). Subsequently, the copper chloride solution was set to pH 8 and added to the ceria suspension to obtain the desired loading. After the addition, the pH value was checked again and adjusted to 9. Then, the reaction mixture was heated at 65 °C for 2 h and placed in an ultrasonic bath for 30 min after cooling. Finally, the residue was centrifuged, washed four times with deionized water, and dried at 85 °C for at least 24 h.

2.2 Catalyst Characterization

Transmission Electron Microscopy (TEM) and Energy-dispersive X-ray (EDX) measurements. TEM measurements were performed on a JEOL JEM-2100F (Tokyo, Japan),

which is equipped with a Schottky field emitter and operates at a nominal acceleration voltage of 200 kV. For preparation, the sample was dispersed in an ultrasonic bath for 30 s in ethanol and then placed on a carbon grid (Plano). After drying, the grid was coated with carbon (Bal-Tec MED010) to prevent charging by the electron beam. EDX spectra were recorded on an Oxford X-MAX 80 silicon drift detector (Oxford Instruments Nanoanalysis, High Wycombe, UK), which is attached to a JEOL JEM-2100F (Tokyo, Japan).

***Operando* Spectroscopy.** The catalytic activity, *operando* Raman (λ_{ex} = 532 nm) and UV-Vis as well as quasi *in situ* XP measurements were performed using an experimental setup that has been described previously.[25,39,50,52,53] Briefly, for the measurements, about 20–25 mg of the sample was placed in a stainless steel sample holder (8 mm diameter, 0.5 mm depth) and the catalyst temperature was set to 130 °C or 190 °C in all measurements. Due to the cell geometry and since the gases flow over the catalyst sample, the amount of catalyst has hardly any influence on the activity when the sample holder is fully covered. The gases CO (99.997%, Westfalen) and argon (99.996%, Westfalen) were dosed by digital mass flow controllers (MFCs, Bronkhorst), while $H_2{}^{16}O$ (electrical conductivity < 3 μSm^{-1}), $H_2{}^{18}O$ (97%+ ^{18}O, Eurisotop) and $D_2{}^{16}O$ (99.9% D, Sigma Aldrich) were dosed by a controlled evaporator mixer (CEM, Bronkhorst) and a liquid mass flow meter (LFM, Bronkhorst). The total flow rate was set to 100 mL/min. All gas compositions were balanced in argon to keep the conversion low and eliminate the influence of possible transport effects, which allowed us to focus on the reaction mechanism. This also applies to the DRIFTS measurements, which will be described below.

The laser power for Raman measurements at the position of the sample was 1 mW, as measured with a power meter (Ophir). Spectra of the catalysts were recorded with an exposure time of 150 s and 3 accumulations. For all measurements a cosmic ray filter and an auto new dark correction were applied, resulting in a total measuring time of about 1800 s for the Cu/CeO_2 catalysts. All Raman spectra reported in this work were normalized to the F_{2g} band, the position of which was determined by curve fitting using Lorentzian functions.

UV-Vis spectra were taken before and after a Raman spectrum and the measuring time was 60 s, resulting from 200 runs with an exposure time of 300 ms each. As white standard, magnesium oxide powder (MgO, Sigma Aldrich) was employed, which shows no absorption between 170 nm and 1100 nm.

To analyze the gas phase and its composition, a Fourier transform infrared (FTIR) spectrometer (Tensor 20, Bruker) was installed at the outlet of the reaction cell. The resolution

was 4 cm^{-1}, and the measurement time was 1 minute, allowing for the accumulation of 125 spectra. Using calibration curves, the concentration of CO_2 was calculated to determine the conversion of CO. The catalytic activity is the ratio of the amount of CO_2, as measured by FTIR at the outlet of the cell, to the amount of dosed CO.

Quasi *in situ* XPS. XP spectra were recorded on a modified LHS/SPECS EA200 MCD system using a Mg Kα source (1253.6 eV, 168 W) as described previously.[50,52,54] The calibration of the binding energy scale was performed with Au $4f_{7/2}$ = 84.0 eV and Cu $2p_{3/2}$ = 932.67 eV signals from foil samples. Prior to the measurements, the sample was treated successively with Ar, H_2O/CO/Ar and H_2O/Ar at 190 °C, and the subsequent transfer of the sample into the analysis chamber was performed without air exposure (quasi *in situ*). To minimize partial charging, the sample was placed on a gold-coated stainless steel sample holder. Further sample charging was taken into account by setting the peak of the C 1s signal to 284.8 eV. Survey spectra were recorded at a resolution of 0.4 eV and detailed spectra at a resolution of 0.025 eV.

Modulation Excitation (ME)-DRIFTS. ME-DRIFTS was performed on an INVENIO spectrometer (Bruker) equipped with a liquid nitrogen–cooled mercury cadmium telluride (MCT) detector and a commercial reaction cell (Praying Mantis™ High Temperature Reaction Chamber, Harrick Scientific Products) with infrared transparent ZnSe windows. Please note, a more detailed description of our basic DRIFTS setup has already been published,[55,56] and the additionally needed MES setup (gas pipelines, communication channels, data processing) is described in [57].

In our measurements, 25–35 mg of the catalyst was placed in a stainless steel sample holder (8 mm Ø, 0.5 mm depth). The exact weight of the sample has hardly any influence on the catalytic activity due to the cell geometry and because the gas flows over the sample. In this context our previous experiments on CO oxidation over Au/ceria catalysts have demonstrated a strong resemblance of the activities obtained in the Raman/UV-Vis setup to those recorded in the DRIFTS setup, with regard to both absolute activities and temporal behavior.[56] As background, the catalyst itself was used after 15 min pretreatment in either H_2O atmosphere (100 mL min^{-1} of 8 vol% H_2O in argon), D_2O atmosphere (100 mL min^{-1} of 8 vol% D_2O in argon) or CO atmosphere (100 mL min^{-1} of 2 vol% CO in argon) at the reaction temperature of 190 °C and a subsequent gas phase modulation procedure (identical to the desired experiment), which ensures a reproducible state of the sample. The atmosphere during the background measurement was the same as in the respective pretreatment. For our measurements we used

the rapid scan mode extension of the spectrometer software OPUS 8.5. Spectra were measured from 850 cm^{-1} to 4000 cm^{-1} with a resolution of 0.2 cm^{-1}, an aperture of 6 mm, and a mirror speed of 120 kHz. A Valco Instruments 4/2 valve (Model E2CA, version ED), communicating with the INVENIO, is used to rapidly switch the gas flows, which are set via digital MFCs (Bronkhorst).

During ME-DRIFTS, the sample is constantly exposed to one of the three feeds already described for the pretreatment. Whereas in the case of constant H_2O and D_2O (both kept at 8 vol%), at the same time a flux of CO is pulsed over the sample, changing from 0 vol% to 2 vol%, in the case of constant CO (kept at 2 vol%), a flux of H_2O or D_2O is pulsed, changing from 0 vol% to 8 vol%. In all cases, the total flow rate is 100 mL min^{-1} balanced with Ar. Switching the valve position initially resulted in a square wave modulation behavior of the modulation gas (CO or H_2O or D_2O) concentration, but due to the residence time behavior of the setup, it is better fitted by a sine wave, as already discussed in our previous work.[57]

One measurement series consisted of 20 periods, with a duration of 292 s each. For each spectrum, five consecutive interferograms were averaged, so that one spectrum is acquired approximately every 3.7 s. This value is also used to approximate the experimental uncertainties of the time values derived from phase-sensitive detection (PSD). For further investigations on the stability of identical successive measurements, please refer to our previous work.[57]

3. Results and Discussion

3.1 Catalyst characterization and performance

Regarding the characterization of the ceria samples, we refer to our previous studies.[39,40,50,51] Briefly, the specific surface areas of sheets, polyhedra, cubes and rods are 57, 36, 32 and 88 m^2g^{-1}, respectively. TEM images of the corresponding particles are provided in ref. [40] (cf. Figure 1). The copper loading was determined by ICP-OES (inductively coupled plasma – optical emission spectrometry) to be 0.42, 0.46, 0.46, and 0.45 wt% for the sheets, polyhedra, cubes, and rods, respectively. Furthermore, no copper was detected by TEM in exemplary measurements on sheets and cubes before and after reaction at 190 °C, the detection of which would be an indication of larger copper clusters (not shown). However, EDX verifies the presence of copper on the entire particles, for both large and small measuring areas (see Figure S1). Hence, the combined electron microscopy results point to the presence of highly dispersed copper on the surface of the ceria particles, in good agreement with the N_2O−CO temperature-programmed desorption (TPD) results of a previous study on similarly prepared Cu/CeO_2 catalysts, which revealed a copper dispersion of 100 % at a loading of 1.9 wt%.[58]

Figure 1 summarizes WGS activities at 130 and 190 °C for the different Cu/CeO_2 catalysts. At both temperatures the same trend in conversion is observed: sheets > polyhedra > cubes > rods. Under these conditions, the bare ceria samples show no significant WGS activity. Interestingly, the activities are very different from those of Cu/CeO_2 catalysts prepared by incipient wetness impregnation (IWI),[59] which is expected to result in lower copper dispersions than the deposition-precipitation (DP) method. According to Figure 1, polyhedra- and sheet-based catalysts gave by far the highest conversions, while for the catalysts in ref. [[59]] prepared by IWI the cubes were more active than the polyhedra, which is consistent with literature results on 5 wt% Cu/CeO_2 catalysts prepared by the DP method.[29] It needs to be mentioned, however, that for the catalysts used in this study, the copper loading was about ten times smaller and thus on average smaller copper clusters are expected to be present on the surface.[29] In any case, the observed differences in reactivity behavior highlight that, besides the preparation method and copper loading, which may both affect the copper dispersion, also the ceria surface termination plays a major role regarding the WGS activity of Cu/CeO_2 catalysts. In this study we will focus on samples prepared by DP, since these samples show slightly higher conversions. In the following, mostly *operando* measurements at 190 °C will be presented to illustrate the largest possible structural changes.

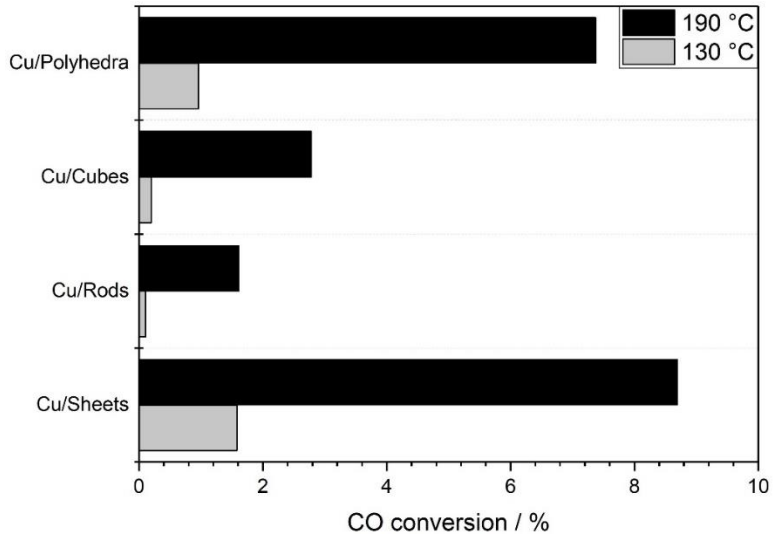

Figure 1. Percentage CO conversion during LT-WGS of Cu/CeO_2 catalysts with different morphologies at 130 °C and 190 °C. The catalytic activity was measured after at least 1 h on stream in 2 vol% CO/8 vol% H_2O/Ar (total flow rate: 100 mL/min).

3.2 Copper State: Dependence on Gas Exposure

To characterize the copper state, we employed quasi *in situ* XP and *operando* UV-Vis spectroscopy. XP spectra were recorded after pretreatment in argon, reaction atmosphere and H_2O at 190 °C (see Figure S2). Due to the small copper loading, only the Cu $2p_{3/2}$ photoemission gave an acceptable signal-to-noise (S/N) ratio. While the binding energies of Cu^0 and Cu^+ hardly differ, the presence of Cu^{2+} can be identified via its slightly shifted binding energy and a shake-up structure, as discussed previously in the context of reference substances (Cu foil, Cu_2O, CuO).[60] Our samples contain finely dispersed copper on ceria, which may show significantly shifted binding energies as a result of metal–support interactions.[61] Additionally, the copper coverage may have an influence on the position of the Cu $2p_{3/2}$ signal.[62] Nevertheless, shake-up structures, which are indicative of Cu^{2+}, are evident at 943 eV, especially for the sheets and polyhedra. In the absence of the reaction mixture, electronic metal–support interactions occur, which are expected to oxidize metallic copper.[42,43] Previous studies have also shown that at low loadings (1 wt% Cu) no metallic copper is present on the surface, even during CO treatment.[43] We therefore attribute the observed Cu $2p_{3/2}$ photoemission to Cu^+ and/or Cu^{2+}, which is underlined by our UV-Vis results discussed next, which allow changes to be detected when switching between different gas environments.

The *operando* UV-Vis spectra in Figure 2 were recorded at 190 °C, successively in argon, reaction atmosphere, water, and argon. All UV-Vis spectra show a dynamical absorption behavior in the visible region, which is generally characterized by Ce^{4+}–Ce^{3+} charge transfer transitions (broad),[63] absorption bands of Cu^+ and/or $[Cu_2O]^{2+}$ species (400–470 nm), and d-d Cu^{2+} transitions (600–850 nm).[64–66] Besides, copper surface plasmons may contribute to the signal (520–580 nm), providing evidence of larger metallic copper domains (Cu_n),[67,68] while highly dispersed metallic copper may not be detectable by UV-Vis.

The samples show clear differences in their absorption behavior (see Figure 2), but it is difficult to make quantitative statements, owing to the width of the bands. The sheets and polyhedra (see Figure 2A) show a significantly higher absorption for wavelengths > 450 nm in argon, which speaks for the presence of Cu^+ and/or $[Cu_2O]^{2+}$ species. In addition, all samples show a band at about 700 nm, which is most pronounced for the sheets but has the highest (and broadest) absorption for the polyhedra. Since previous studies provided no evidence of metallic copper on low-loaded Cu/CeO_2,[43] this band can be assigned to Cu^{2+}.[65] The observations indicate significant differences in the copper species under argon, whereby the 111 surfaces possess the highest fraction of Cu^+ and Cu^{2+} on the surface, consistent with our XPS results.

When switching to reaction conditions, all samples show a broad increase in absorbance at wavelengths above 450 nm, indicating a reduction of the support. When CO is switched off, this absorption feature decreases again; in the case of the polyhedra and sheets, it becomes even lower than that detected in the argon phase prior to reaction conditions. The width of the feature may suggest that the sheets and polyhedra are more oxidized than in the initial argon phase, in contrast to the rods and cubes, which do not show any significant changes in the spectral profile.

To check the stability of the catalysts, we compared the UV-Vis spectra in argon before and after applying reaction conditions. Figure 2B reveals that the rods and cubes do not undergo any changes, while the sheets and polyhedra show a slightly higher absorption over the entire visible range. Especially for the sheets this is noticeable in the region around 700 nm and may be indicative of an increase in Cu^{2+} species. Interestingly, in a direct comparison with our previous results on Au/CeO_2 catalysts with similar noble metal loadings, where the increase in Vis absorption from one argon phase to the other correlated negatively with the activity,[39,40] the Cu/CeO_2 samples show an inverse behavior (see also below). In the case of the gold samples, we could attribute the observed behavior to gold agglomeration. For the copper samples, agglomeration is unlikely, as it would lead to lower activities over time, which is not consistent with our results. We therefore attribute the observed UV-Vis behavior to an increase in the amount of Cu^{+} and Cu^{2+} surface species.

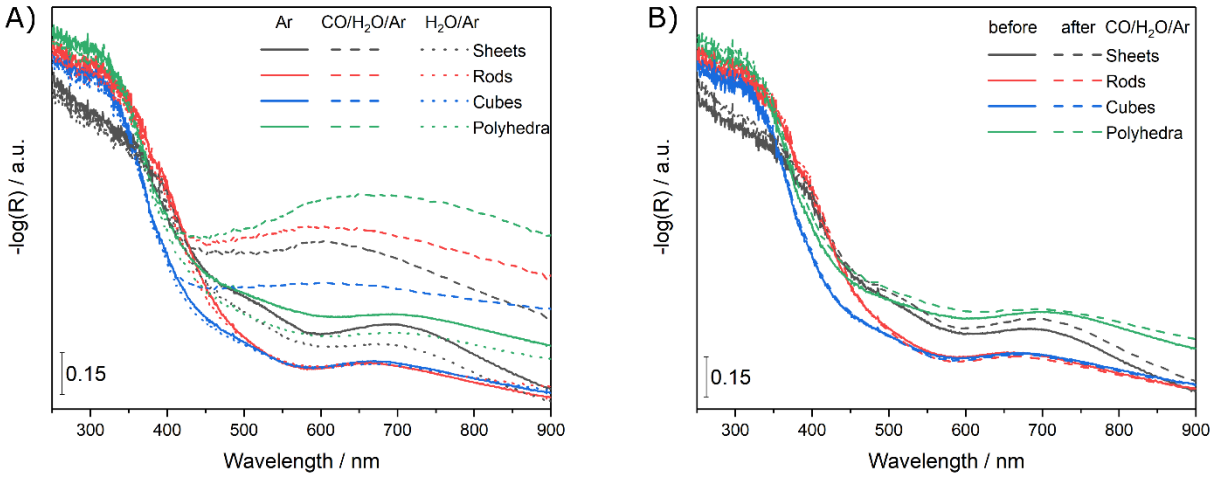

Figure 2. *In situ* / *operando* UV-Vis reflectance spectra of Cu/CeO_2 sheets (black), rods (red), cubes (blue), and polyhedra (green) at 190 °C **A)** for different gas exposures, **B)** before and after reaction conditions.

3.3. Structural Dynamics Under Reaction Conditions

For better visualization of the dynamic changes in the UV-Vis spectra, Figure 3A shows the absorbances at 700 nm under different gas atmospheres at 130 and 190 °C. There is a clear dependence on the gas-phase composition and temperature. All samples reach their maximum absorption under reaction atmosphere and show a reversible behavior in H_2O or argon, as already indicated in Figure 2.

At 190 °C, the absolute increases are slightly higher than at 130 °C, but vary significantly between the samples. Figure 3B depicts the negative correlation between the differences in CO conversion and the absorbances under reaction conditions at the two temperatures, showing a near-linear behavior. As mentioned above, the broad increase in absorption is mainly due to the reduction of the support materials. Considering that there is no relation between the CO conversions and specific surface areas, we can conclude that defects are only a minor factor in determining the catalytic activity; thus, a surface too rich in defects (e.g. rods) may not be beneficial for WGS over Cu/CeO_2. This is further supported by the observation that the absolute change in absorption upon switching from argon to reaction conditions does not correlate with the WGS activity, consistent with previous results on CO oxidation, which have shown that the Ce^{3+} fraction is not correlated with activity and that the state of copper is of greater importance.[42]

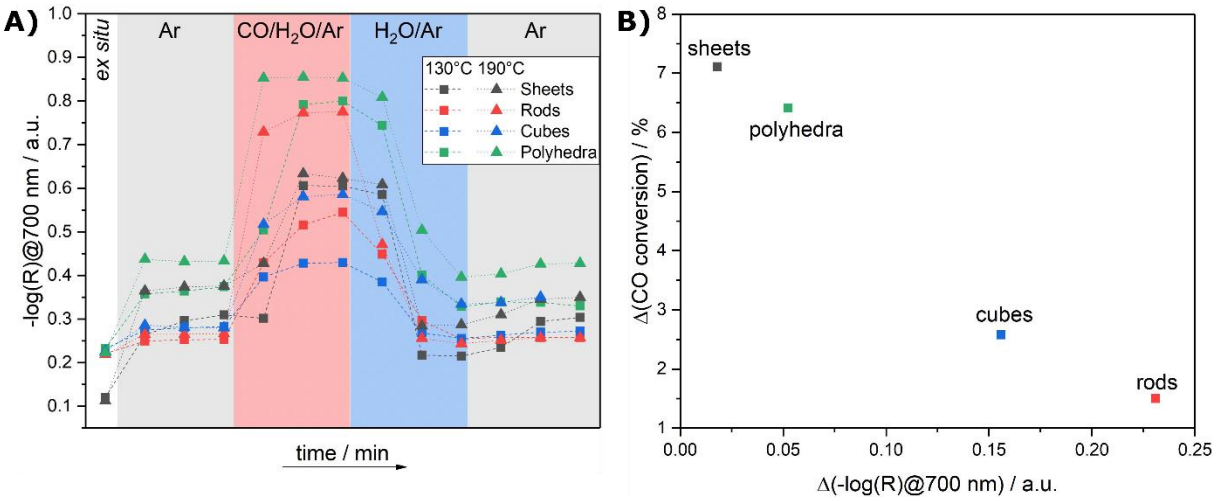

Figure 3. A) *In situ* / *operando* UV-Vis results for Cu/CeO_2 catalysts recorded during the indicated gas exposures at 130 °C (square) and 190 °C (triangle) and at a total flow rate of 100 mL/min, except for the *ex situ* spectra, which were taken at 25 °C. Spectra were recorded at the beginning, after about 30 min, and after about 1 h of exposure to the indicated gas phases. **B)** Correlation of the difference in CO conversion at 190 and 130 °C with the difference in

absorbance at 700 nm, determined approximately 1 h after beginning to apply reaction conditions.

Next, the results from Raman spectroscopy at 532 nm excitation will be discussed. In the context of ceria-based catalysts, the F_{2g} band provides important information about the oxygen dynamics, as shown previously.[39,50,53] Figure 4A depicts the F_{2g} shifts when switching from the first argon to the reaction phase. In addition, as part of the measurements, isotope labelling by $H_2{}^{18}O$ was used to follow the exchange of lattice oxygen by H_2O. As discussed previously, at constant temperature, the F_{2g} shift allows changes in the defect density of the support to be monitored.[50] The gas phase–dependent F_{2g} positions (see Figure S3) show a behavior similar to that described in the context of the UV-Vis data in Figure 3. However, absolute changes differ from those in the UV-Vis spectra. For example, the polyhedra show the highest absorption in the UV-Vis measurements, while the F_{2g} red-shift is lowest after the sheets. This behavior may be explained either by additional copper contributions to the UV-Vis spectra, which dominate the Ce^{4+}–Ce^{3+} charge transfer transitions, or by the different penetration depths of the two methods. Closer inspection of the F_{2g} shifts in Figure 4A when using $H_2{}^{16}O$ under reaction conditions (blue bar) reveals the following trend regarding the F_{2g} red-shift: sheets < polyhedra < cubes < rods. Thus, the sheets are reduced the least, while the rods are reduced the most. As the same trend is also observed for $H_2{}^{18}O$ (black bar), the same applies to the replacement of lattice oxygen by ^{18}O. Interestingly, the absolute F_{2g} shifts at 130 °C (not shown) are identical to those at 190 °C despite the lower activity, which is a clear indication that the catalytic activity is not linked to the support reducibility. This is further supported by the negative correlation of the F_{2g} shifts with the CO conversions, shown in Figure 4B. Based on the above findings from *in situ* / *operando* Raman spectroscopy, we can exclude a mechanism that is only linked to the reducibility, fully consistent with the UV-Vis results.

From the Raman spectra during reaction conditions and $H_2{}^{16}O$ exposure (see Figure S4) it is difficult to extract further information besides the F_{2g} position, owing to self-absorption (see UV-Vis results) and fluorescence effects. An exception is the detection of a feature at around 1560 cm^{-1} for the polyhedra and cubes, which becomes even more obvious at 130 °C (see Figure S5) and may indicate the presence of carbonates. For unloaded samples this band is not observed (not shown). Adsorbate signals will be discussed in more detail below in the context of the DRIFTS measurements.

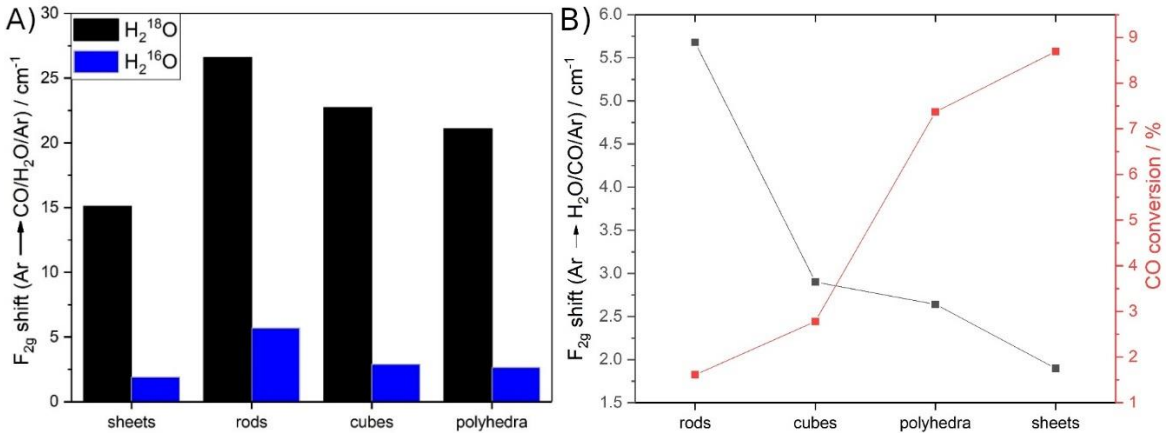

Figure 4. *In situ* / *operando* Raman spectroscopic results (532 nm) showing the **A)** F_{2g} shifts of Cu/CeO_2 catalysts when switching from argon atmosphere to reaction conditions (CO/H_2O/Ar; flow rate: 100 mL/min) using $H_2{}^{16}O$ (blue) and $H_2{}^{18}O$ (black), **B)** correlation between F_{2g} shifts and CO conversion.

An important aspect regarding the functioning of ceria-based catalysts is the mobility of lattice oxygen and/or oxygen vacancies. To this end, it should be pointed out that all samples exhibit an F_{2g} blue-shift when switching from reaction conditions to $H_2{}^{16}O$ (see Figure S3), demonstrating that the support is oxidized by water. Interestingly, for $H_2{}^{18}O$ a different behavior is observed. This is illustrated by Figure 5, which depicts the F_{2g} positions during the different gas phases at 190 °C. It is noticeable that polyhedra and cubes do not undergo any changes in the F_{2g} position after reaction conditions, while the F_{2g} positions of the sheets and rods show blue-shifts of 11.7 and 4.8 cm^{-1}, respectively. Compared with the blue-shifts detected after reaction conditions in the case of $H_2{}^{16}O$, these shifts are significantly larger for the sheets (3.0 cm^{-1}) and slightly smaller for the rods (5.4 cm^{-1}). Before discussing the observed behavior, we will briefly summarize the different contributions to the F_{2g} shifts. The reduction of the support and the exchange of ^{16}O by ^{18}O leads to a red-shift, while the opposite processes, i.e., the oxidation or the exchange of ^{18}O by ^{16}O, lead to blue-shifts. Since each sample undergoes oxidation (accompanied by a blue-shift) upon switching from reaction conditions to $H_2{}^{16}O$ flow, there must be a further exchange of ^{16}O with ^{18}O by $H_2{}^{18}O$ for the polyhedra and cubes, which compensates the blue-shift due to support oxidation. For the rods a blue-shift is observed, which may originate from oxidation and/or diffusion of ^{16}O from the bulk to the (sub)surface. We propose that in the case of the rods further exchange of ^{16}O with ^{18}O (from $H_2{}^{18}O$) plays a minor role in contrast to the cubes and polyhedra, since the difference in the comparison of the use of $H_2{}^{16}O$ and $H_2{}^{18}O$ and the absolute shift between reaction conditions and the subsequent H_2O

phase is less than 1 cm^{-1}. For the sheets the blue-shift is by 8.7 cm^{-1} larger than that detected as a result of oxidation during the $H_2{}^{16}O$ experiments. Remarkably, this behavior reveals that the ceria sheets facilitate the transport of ^{16}O from the bulk to the (sub)surface. In this context, it should be pointed out that the red-shift under reaction conditions is smallest for the sheets and thus most of the ^{16}O is still present. In contrast, the polyhedra, which come closest to the sheets regarding the F_{2g} shifts, exhibit a completely different behavior, as mentioned above. Thus, the ceria sheets are the only support material that shows a high mobility of lattice oxygen and/or oxygen vacancies, probably contributing to its high activity, while surface area related effects can be excluded, since, for example, the rods have a larger surface area than the sheets.

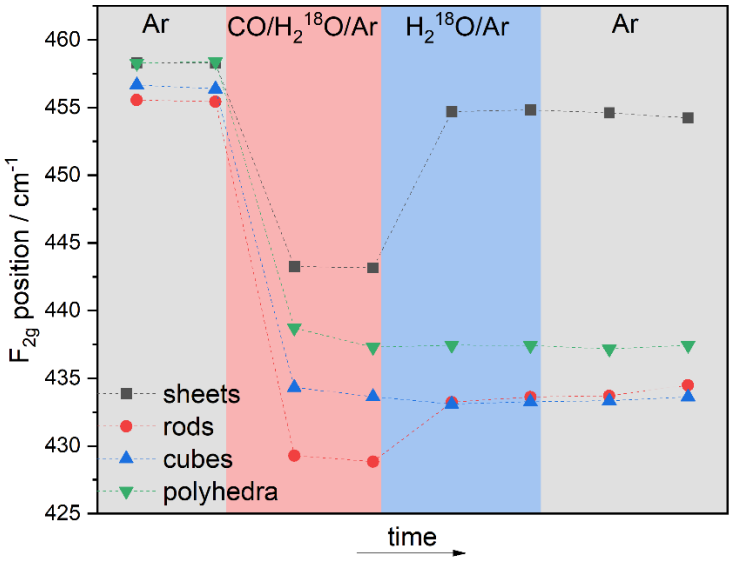

Figure 5. *In situ* / *operando* Raman F_{2g} positions for Cu/CeO_2 catalysts exposed to the indicated gas environments at 190 °C using $H_2{}^{18}O$ (total flow rate: 100 mL/min). The underlying spectra were recorded at 532 nm excitation and after gas-phase exposure for about 30 min and 1 h.

ME-DRIFTS experiments were conducted to explore the adsorbate dynamics and to assess the possibility of an associative mechanism. As potential adsorbates participating in the reaction, carbonates (850–1800 cm^{-1}), CO adsorbates (2000–2200 cm^{-1}), and hydroxyls (3400–3800 cm^{-1}) may be expected. Figure 6 depicts the complete PSD spectra of a CO pulse experiment (i.e., switching between 0 and 2 vol%) with a constant flow of 8 vol% H_2O/Ar over Cu/CeO_2 sheets. The same type of experiments was also performed for the other Cu/CeO_2 samples as well as the bare supports (see Figures S6 and S7), revealing a similar overall behavior despite differences in the spectral profiles. In Figure 6, the carbonate region is characterized by signals at 1009, 1285, 1388, 1434, 1470, 1547 and 1597 cm^{-1}. The most intense

signals, at 1285 and 1597 cm^{-1}, are attributed to the presence of bidentate carbonate,[50,69] while the residual features originate from other carbonate-like species, e.g. bridged formate species.[69,70] Notably, in the CO region no signals are detected, except the contributions of gaseous CO (see Figure S8). To this end, our previous studies have demonstrated that the sensitive detection of adsorbed CO is not limited by the presence of the gas-phase CO signature.[57] Thus, based on our findings from transient ME-DRIFTS-PSD, a major contribution of CO adsorbates to the WGS reaction can be ruled out. This is in accordance to an *in situ* (steady state) DRIFTS study on low-loaded Cu/CeO_2, which did not report any CO adsorbates above 150 °C.[36] Even enhancing the time resolution in another series of experiments, in which spectra were recorded every 0.5 s, did not lead to the appearance of any CO-related adsorbate signals. Inverting the modulation sequence by switching H_2O (between 0 and 8 vol%) at a constant flow of 2 vol% CO/Ar reveals a minor signal at around 2109 cm^{-1}, which is characteristic of Cu^+-CO species (see Figure S8 for enlarged view and Table S1).[71] Considering that the signal is small and only appears in modulation experiments favoring its presence, we propose CO adsorbates to have a negligible (if any) role in the WGS reaction. To further clarify this behavior, we also performed steady-state DRIFTS measurements on the sheets (see Figure S11). These clearly show that a band is visible at 2109 cm^{-1} under CO/Ar, but decreases significantly under reaction conditions. The electronic contribution[72] at 2025 cm^{-1} remains constant, which is why it does not appear in the ME-DRIFTS experiments. Thus, the steady-state results are fully consistent with our ME-DRIFTS results.

The hydroxyl region contains signals at 3530, 3622, 3642, and 3653 cm^{-1}, as well as contributions of combination bands of gaseous CO_2 centered at about 3610 and 3710 cm^{-1}.[73] The hydroxyl feature at 3620 cm^{-1} is attributed to a triply bonded OH group (type III),[74] while those at 3642 and 3653 cm^{-1} are associated with OH (type II-B) and OH (type II*-B),[75] which may mutually transform into each other (see below). The assignment of the 3530 cm^{-1} feature is less obvious. Previously, OH features within 3520–3660 cm^{-1} have been assigned to bi- and tri-coordinated species,[76] also consistent with our other hydroxyl assignments.

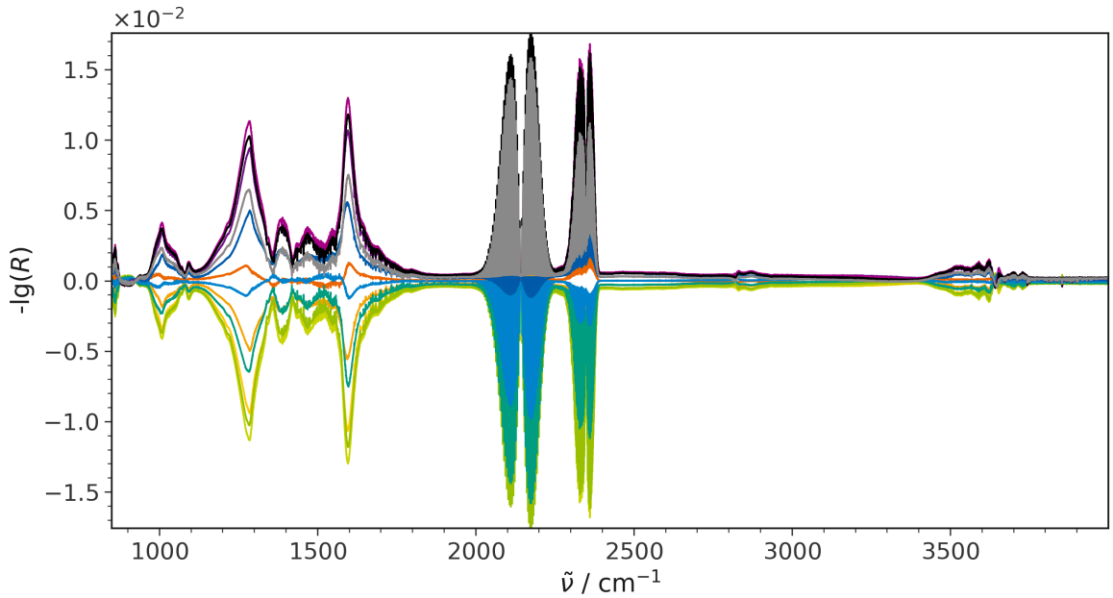

Figure 6. PSD spectra of Cu/CeO_2 sheets at 190 °C. The gas-phase composition was periodically changed from 8 vol% H_2O/Ar to 2 vol% CO/8 vol% H_2O/Ar.

From the PSD spectra, time values were determined, which show the sequence of signals within one (modulation) period, thus yielding important mechanistic information (see Table 1). The first two signals that appear correspond to the CO reactant (~23 s) and the product CO_2 (~40 s), while the signals within the carbonate region show larger time values (45–50 s), as do the hydroxides at 3530 and 3622 cm^{-1}. The OH signal at 3653 cm^{-1} (II*-B) increases and that at 3642 cm^{-1} (II-B) decreases in the more reductive phase (i.e., during CO pulsing), as would be expected (see Table 1). On the other hand, as these signals are expected to mutually transform into each other, it appears surprising at first that they do not appear at exactly the same time value (with opposite sign). The observed deviation may originate from their overlap with other signals, thereby mixing up their time values, as has been discussed in more detail previously.[57]

Taking into account the experimental uncertainty of 3.7 s for the time values, none of the species observed in the carbonate and hydroxide region may take part in the initial formation of the product CO_2.

Table 1. Results from transient IR-PSD analysis of Cu/CeO_2 sheets. Time values correspond to the signal onset, and signals of decreasing bands are marked with (-). Refer to Figure 6 for the underlying PSD spectra.

Position / cm^{-1}	t(Cu/CeO_2) / s	Assignment
3653	73	OH (II*-B)
3642	46 (-)	OH (II-B)
3622	45	OH (III)
3530	45	OH (type III)
2361	40	CO_2 (g)
2064	23	CO (g)
1597	45	Bidentate carbonate
1547	50	Carbonate species
1470	48	Carbonate species
1434	49	Carbonate species
1388	50	Carbonate species
1285	45	Bidentate carbonate
1009	46	Bidentate carbonate

To identify signals of catalytically active species, we follow a routine comprising three main steps. In the first step, spectator signals are removed by subtracting a background spectrum of a catalyst that has already undergone several modulation periods prior to the actual modulation experiment and by applying a PSD to the recorded data set. In the second step, we characterize the species that appear in PSD spectra as a result of the periodic (precursor) concentration changes according to their temporal behavior. For a consistent picture, the comparison of PSD spectra from different reactant modulation schemes is crucial, as catalytically active species are expected to appear in both data sets and at comparable times.

Following our routine, additional ME-DRIFTS experiments were performed, in which now the 2 vol% CO/Ar flow was kept constant and water was periodically pulsed, thus switching from 0 to 8 vol% share of the total flow (see Figure S9). A comparison of the spectra obtained with both modulation approaches (pulsing CO or H_2O) is shown in Figure S10. At this point it should be noted that both cases lead to similar CO_2 conversions, since both modulation conditions result in the same (dynamic) conditions that enable the WGS reaction. Temporal analysis reveals that all of the detected signals appear or disappear more or less at the same time as the pulsed H_2O component, except those of CO_2 or weakly adsorbed H_2O, which are delayed by ~3–5 s (see Table S1). In the hydroxyl region, clear signals are missing (see Figure S10), suggesting that there are no actively participating hydroxyls involved in H_2 formation. It should be mentioned, however, that weak hydroxyl signals may be masked by contributions from gaseous and weakly adsorbed water in that spectral region. Besides, the possibility of a highly labile and fast-reacting hydroxyl species, as suggested previously, cannot be excluded.[36] When comparing the combined results from the modulation experiments, there is no spectroscopic evidence that would unambiguously point towards an associative mechanism. Although some

adsorbate signals are observable in the spectra of both modulation experiments (see Figure S10), the temporal analysis reveals that all adsorbate signals in the CO modulation experiment are observed after product formation (see Table 1), while in the case of H_2O modulation, signals appear slightly earlier than product formation (see Table S1). Therefore, the observed behavior may be described by adsorption / desorption processes taking place when the respective reactant CO or H_2O is pulsed over the surface, rather than a direct participation in the reaction.

The bidentate carbonate pattern observed in Figure 6 did not appear when H_2O was pulsed (see Figure S9), which was further confirmed by D_2O pulsing experiments aiming at a carbonate region less crowded by gaseous water. Although these experiments cleared the view for the carbonate region, the findings from our H_2O measurements were confirmed, i.e., that there is no signal of an active species that might be attributed to CO_2 formation.

4. Discussion of the Reaction Mechanism

In the literature, two main mechanisms have been proposed for the WGS reaction over metal-supported oxide catalysts: a redox mechanism and an associative one. The latter proceeds via intermediates, e.g. carbonates, formates, or hydroxides.[30,31,77] Furthermore, theoretical studies on pure CeO_2(111) show a combined redox–associative route.[78] It has been challenging to find *operando* approaches that enable a critical assessment of the reaction mechanism. Here we propose a spectroscopic approach based on the combination of *operando* and transient methods. In this context it should be mentioned that the type of mechanism depends on the properties of the catalyst system as well as on the temperature.

Based on our spectroscopic findings, we identified several catalyst properties that may be related to the activity of the catalyst. These include the reducibility, whose dynamics could be followed by means of *operando* Raman and UV-Vis measurements; the mobility of lattice oxygen, which could be detected by the $H_2{}^{18}O$ Raman experiments; and the tendency to form stable adsorbates (e.g. surface carbonates), which may block active sites. The last property is of particular relevance for the 110 and 100 surface (rods and cubes), as demonstrated previously by CO-TPD for bare octahedra, cubes, and rods,[79] and by Raman/UV-Vis spectroscopy for low-loaded Au/CeO_2.[39] In addition, from our transient spectra, there is no evidence for the presence of intermediates on either the support or copper, which would have supported an associative mechanism. Instead, our results are in agreement with a redox mechanism, consistent with our previous studies on Au/CeO_2 catalysts.[25,39]

The *operando* Raman results have revealed a negative correlation of the F_{2g} shift with the conversion (see Figure 4B), demonstrating that the reducibility is not directly responsible for

the activity. Based on the assumption of a redox mechanism, this finding may be related to the fact that oxygen must be available at the surface to allow for facile oxidation of CO. To this end, the isotope experiments have shown that in the case of sheets, oxygen is readily supplied to the surface for CO oxidation. We therefore propose the superior LT-WGS performance of the sheet-based catalysts to be related to the availability of surface oxygen. In fact, for the less active polyhedra, a significantly lower diffusion of oxygen (vacancies) from bulk to surface was observed (see Figure 5). For the cubes and rods, on the other hand, the reducibility is too high, leading to an enhanced reactivity towards CO_2 and the formation of surface carbonates, which may block active sites.

The comparison of loaded and unloaded samples clearly shows that the presence of copper plays a major role, since none of the ceria supports exhibit any LT-WGS activity. To this end, besides the specification of the copper oxidation state, the role of copper in the mechanism is of importance. Starting with the last point, our transient DRIFTS measurements provide no indication for an active involvement of copper in the reaction. While we cannot exclude hydrogen recombination occurring so rapidly that it cannot be detected despite the use of a transient method, we rather propose copper to change the electronic properties. This is supported by the *operando* UV-Vis spectra, since, for example, the unloaded sheets and polyhedra (not shown) do not show any significant changes in the visible range in contrast to the loaded samples. Thus, the presence of even small loadings of copper significantly changes the reduction properties. This is also supported by the Raman spectra, which do not show significant F_{2g} red-shifts under reaction conditions.[39]

Regarding the oxidation state of copper, our UV-Vis and XPS results suggest that the surface termination plays a role. In particular, the 111 surfaces were found to exhibit a larger fraction of Cu^{2+} on the surface, which we postulate as a possible reason for the higher activities of the polyhedra and sheets.

In summary, our results are consistent with a redox mechanism in which oxidation occurs by water, with oxygen being incorporated into the crystal lattice. This process is so fast that no intermediates are observed. Finally, reduction takes place by CO, which immediately reacts to CO_2.

5. Conclusions

In this work, we demonstrate the use of a combined operando/transient spectroscopic approach to investigate the redox properties and the intermediate/adsorbate dynamics on supported metal catalysts. We address low-loaded Cu/CeO_2 catalysts during LT-WGS reaction, providing first

evidence for a pure redox mechanism using coupled *operando* Raman and UV-Vis spectroscopy, which in turn is supported by transient ME-DRIFTS experiments. Thus, information about bulk CeO_2 can be obtained using Raman and UV-Vis spectroscopy, while UV-Vis spectra provide additional information about dispersed copper species. ME-DRIFTS measurements are used to identify surface intermediates. To explore the facet-dependent behavior, ceria sheets (111, steps), polyhedra (111), cubes (100), and rods (110, 100) are studied.

Summarizing the key findings, there is no direct correlation between activity and reducibility based on the conversion data and the *operando* Raman and UV-Vis results, while the use of $H_2{}^{18}O$ experiments underlines the importance of transport properties and the availability of oxygen at the surface. Regarding surface processes, our transient DRIFTS measurements do not show any active participation of copper or adsorbates in the WGS reaction; while the presence of various surface carbonates is observed, temporal analysis reveals their role as spectator species. However, it should be noted, that highly reactive surface intermediates cannot be completely excluded, despite the also previously shown high sensitivity of ME-DRIFTS.[50,57]

With respect to copper, we can conclude that its participation in the catalysis is mainly based on electronic effects. Such observations have also been reported in previous studies on Cu/CeO_2 catalysts for various reactions.[41] Even small amounts of copper (<0.5 wt%) affect the support properties, inducing significant catalytic activities resulting from metal–support interactions. In contrast to our earlier RWGS study over Au/CeO_2, no intermediates (e.g., carbonates, hydroxides, formates) are involved in the reaction. Furthermore, unlike our gold catalysts from previous studies, Cu/CeO_2 is expected to be more stable, as *operando* Raman and UV-Vis did not give any indication of copper agglomeration. Thus, while gold catalysts may show a somewhat higher activity, they are more expensive and suffer from instabilities.

Our combination of *operando* Raman/UV-Vis spectroscopy and ME-DRIFTS is a powerful tool to investigate a wide range of metal-supported oxide catalysts and to provide a detailed understanding of their functioning, for example, in C1 processes such as RWGS. In particular, our approach allows us to distinguish between redox and associative mechanisms and to investigate their respective weight, which is of great importance to provide new approaches towards better catalysts and, ultimately, to design catalysts based on a profound knowledge of their structural behavior under working conditions.

Supporting Information

Additional characterization data, *in situ/operando* Raman results, quasi *in situ* XPS spectra, additional ME-DRIFTS as well as steady-state DRIFTS data. This information is available free of charge on the ACS Publications website.

Acknowledgements

We thank Stefan Lauterbach and Hans-Joachim Kleebe for TEM and EDX measurements, Martin Brodrecht for BET measurements, and Karl Kopp for technical support and helpful discussions on the XPS results. Jakob Weyel gratefully acknowledges a scholarship from the Fonds der Chemischen Industrie im Verband der Chemischen Industrie e.V.

Conflict of Interest

The authors declare no conflict of interest.

References

(1) Staffell, I.; Scamman, D.; Velazquez Abad, A.; Balcombe, P.; Dodds, P. E.; Ekins, P.; Shah, N.; Ward, K. R. The Role of Hydrogen and Fuel Cells in the Global Energy System. *Energy Environ. Sci.* **2019**, *12* (2), 463–491. https://doi.org/10.1039/C8EE01157E.

(2) Trimm, D. L. Minimisation of Carbon Monoxide in a Hydrogen Stream for Fuel Cell Application. *Appl. Catal. A Gen.* **2005**, *296* (1), 1–11. https://doi.org/10.1016/j.apcata.2005.07.011.

(3) Ratnasamy, C.; Wagner, J. P. Water Gas Shift Catalysis. *Catal. Rev.* **2009**, *51* (3), 325–440. https://doi.org/10.1080/01614940903048661.

(4) Rodriguez, J. A.; Grinter, D. C.; Liu, Z.; Palomino, R. M.; Senanayake, S. D. Ceria-Based Model Catalysts: Fundamental Studies on the Importance of the Metal-Ceria Interface in CO Oxidation, the Water-Gas Shift, CO_2 Hydrogenation, and Methane and Alcohol Reforming. *Chem. Soc. Rev.* **2017**, *46* (7), 1824–1841. https://doi.org/10.1039/c6cs00863a.

(5) Xu, J.; Yang, W.; Song, S.; Zhang, H. Ultra-Small Noble Metal Ceria-Based Catalytic Materials: From Synthesis to Application. *Eur. J. Inorg. Chem.* **2021**, *2021* (8), 689–701. https://doi.org/10.1002/ejic.202000885.

(6) Abdel-Mageed, A. M.; Chen, S.; Fauth, C.; Häring, T.; Bansmann, J. Fundamental Aspects of Ceria Supported Au Catalysts Probed by In Situ/Operando Spectroscopy and TAP Reactor Studies. *ChemPhysChem* **2021**, *22* (13), 1302–1315. https://doi.org/10.1002/cphc.202100027.

(7) Shido, T.; Iwasawa, Y. Regulation of Reaction Intermediate by Reactant in the Water-Gas Shift Reaction on CeO_2, in Relation to Reactant-Promoted Mechanism. *J. Catal.* **1992**, *136* (2), 493–503. https://doi.org/10.1016/0021-9517(92)90079-W.

(8) Kalamaras, C. M.; Dionysiou, D. D.; Efstathiou, A. M. Mechanistic Studies of the Water–Gas Shift Reaction over $Pt/Ce_xZr_{1-x}O_2$ Catalysts: The Effect of Pt Particle Size and Zr Dopant. *ACS Catal.* **2012**, *2* (12), 2729–2742. https://doi.org/10.1021/cs3006204.

(9) Leppelt, R.; Schumacher, B.; Plzak, V.; Kinne, M.; Behm, R. Kinetics and Mechanism of the Low-Temperature Water–Gas Shift Reaction on Au/CeO_2 Catalysts in an Idealized Reaction Atmosphere. *J. Catal.* **2006**, *244* (2), 137–152. https://doi.org/10.1016/j.jcat.2006.08.020.

(10) Goguet, A.; Meunier, F. C.; Tibiletti, D.; Breen, J. P.; Burch, R. Spectrokinetic Investigation of Reverse Water-Gas-Shift Reaction Intermediates over a Pt/CeO_2 Catalyst. *J. Phys. Chem. B* **2004**, *108* (52), 20240–20246. https://doi.org/10.1021/jp047242w.

(11) Meunier, F. C.; Tibiletti, D.; Goguet, A.; Reid, D.; Burch, R. On the Reactivity of Carbonate Species on a Pt/CeO_2 Catalyst under Various Reaction Atmospheres: Application of the Isotopic Exchange Technique. *Appl. Catal. A Gen.* **2005**, *289* (1), 104–112. https://doi.org/10.1016/j.apcata.2005.04.018.

(12) Mudiyanselage, K.; Senanayake, S. D.; Feria, L.; Kundu, S.; Baber, A. E.; Graciani, J.; Vidal, A. B.; Agnoli, S.; Evans, J.; Chang, R.; Axnanda, S.; Liu, Z.; Sanz, J. F.; Liu, P.; Rodriguez, J. A.; Stacchiola, D. J. Importance of the Metal–Oxide Interface in Catalysis: In Situ Studies of the Water–Gas Shift Reaction by Ambient-Pressure X-ray Photoelectron Spectroscopy. *Angew. Chem. Int. Ed.* **2013**, *52* (19), 5101–5105. https://doi.org/10.1002/anie.201210077.

(13) Chen, Y.; Wang, H.; Burch, R.; Hardacre, C.; Hu, P. New Insight into Mechanisms in Water-Gas-Shift Reaction on $Au/CeO_2(111)$: A Density Functional Theory and Kinetic Study. *Faraday Discuss.* **2011**, *152*, 121–133. https://doi.org/10.1039/c1fd00019e.

(14) Vecchietti, J.; Bonivardi, A.; Xu, W.; Stacchiola, D.; Delgado, J. J.; Calatayud, M.; Collins, S. E. Understanding the Role of Oxygen Vacancies in the Water Gas Shift

Reaction on Ceria-Supported Platinum Catalysts. *ACS Catal.* **2014**, *4* (6), 2088–2096. https://doi.org/10.1021/cs500323u.

(15) Liu, Z. P.; Jenkins, S. J.; King, D. A. Origin and Activity of Oxidized Gold in Water-Gas-Shift Catalysis. *Phys. Rev. Lett.* **2005**, *94* (19), 1–4. https://doi.org/10.1103/PhysRevLett.94.196102.

(16) Bobadilla, L. F.; Santos, J. L.; Ivanova, S.; Odriozola, J. A.; Urakawa, A. Unravelling the Role of Oxygen Vacancies in the Mechanism of the Reverse Water–Gas Shift Reaction by Operando DRIFTS and Ultraviolet–Visible Spectroscopy. *ACS Catal.* **2018**, *8* (8), 7455–7467. https://doi.org/10.1021/acscatal.8b02121.

(17) Fu, Q.; Saltsburg, H.; Flytzani-Stephanopoulos, M. Active Nonmetallic Au and Pt Species on Ceria-Based Water-Gas Shift Catalysts. *Science (80-.).* **2003**, *301* (5635), 935–938. https://doi.org/10.1126/science.1085721.

(18) Bunluesin, T.; Gorte, R. J.; Graham, G. W. Studies of the Water-Gas-Shift Reaction on Ceria-Supported Pt, Pd, and Rh: Implications for Oxygen-Storage Properties. *Appl. Catal. B Environ.* **1998**, *15* (1–2), 107–114. https://doi.org/10.1016/S0926-3373(97)00040-4.

(19) Shido, T.; Iwasawa, Y. Reactant-Promoted Reaction Mechanism for Water-Gas Shift Reaction on Rh-Doped CeO_2. *J. Catal.* **1993**, *141* (1), 71–81. https://doi.org/10.1006/jcat.1993.1119.

(20) Burch, R.; Goguet, A.; Meunier, F. C. A Critical Analysis of the Experimental Evidence for and against a Formate Mechanism for High Activity Water-Gas Shift Catalysts. *Appl. Catal. A Gen.* **2011**, *409–410*, 3–12. https://doi.org/10.1016/j.apcata.2011.09.034.

(21) Chen, Y.; Cheng, J.; Hu, P.; Wang, H. Examining the Redox and Formate Mechanisms for Water–Gas Shift Reaction on Au/CeO_2 Using Density Functional Theory. *Surf. Sci.* **2008**, *602* (17), 2828–2834. https://doi.org/10.1016/j.susc.2008.06.033.

(22) Tibiletti, D.; Amieiro-Fonseca, A.; Burch, R.; Chen, Y.; Fisher, J. M.; Goguet, A.; Hardacre, C.; Hu, P.; Thompsett, D. DFT and in Situ EXAFS Investigation of Gold/Ceria-Zirconia Low-Temperature Water Gas Shift Catalysts: Identification of the Nature of the Active Form of Gold. *J. Phys. Chem. B* **2005**, *109* (47), 22553–22559. https://doi.org/10.1021/jp054576s.

(23) Rodriguez, J. A.; Liu, P.; Hrbek, J.; Evans, J.; Pérez, M. Water Gas Shift Reaction on Cu and Au Nanoparticles Supported on CeO_2(111) and ZnO(0001): Intrinsic Activity and Importance of Support Interactions. *Angew. Chem. Int. Ed.* **2007**, *46* (8), 1329–

1332. https://doi.org/10.1002/anie.200603931.

(24) Fonseca, A. A.; Fisher, J. M.; Ozkaya, D.; Shannon, M. D.; Thompsett, D. Ceria-Zirconia Supported Au as Highly Active Low Temperature Water-Gas Shift Catalysts. *Top. Catal.* **2007**, *44* (1–2), 223–235. https://doi.org/10.1007/s11244-007-0295-7.

(25) Schilling, C.; Hess, C. Elucidating the Role of Support Oxygen in the Water–Gas Shift Reaction over Ceria-Supported Gold Catalysts Using Operando Spectroscopy. *ACS Catal.* **2019**, *9* (2), 1159–1171. https://doi.org/10.1021/acscatal.8b04536.

(26) Wang, X.; Rodriguez, J. A.; Hanson, J. C.; Gamarra, D.; Martínez-Arias, A.; Fernández-García, M. In Situ Studies of the Active Sites for the Water Gas Shift Reaction over Cu-CeO_2 Catalysts: Complex Interaction between Metallic Copper and Oxygen Vacancies of Ceria. *J. Phys. Chem. B* **2006**, *110* (1), 428–434. https://doi.org/10.1021/jp055467g.

(27) Barrio, L.; Estrella, M.; Zhou, G.; Wen, W.; Hanson, J. C.; Hungría, A. B.; Hornés, A.; Fernández-García, M.; Martínez-Arias, A.; Rodriguez, J. A. Unraveling the Active Site in Copper-Ceria Systems for the Water-Gas Shift Reaction: In Situ Characterization of an Inverse Powder CeO_{2-x}/CuO-Cu Catalyst. *J. Phys. Chem. C* **2010**, *114* (8), 3580–3587. https://doi.org/10.1021/jp910342b.

(28) Cámara, A. L.; Chansai, S.; Hardacre, C.; Martínez-Arias, A. The Water–Gas Shift Reaction over CeO_2/CuO: Operando SSITKA–DRIFTS–Mass Spectrometry Study of Low Temperature Mechanism. *Int. J. Hydrogen Energy* **2014**, *39* (8), 4095–4101. https://doi.org/10.1016/j.ijhydene.2013.05.087.

(29) Ren, Z.; Peng, F.; Li, J.; Liang, X.; Chen, B. Morphology-Dependent Properties of Cu/CeO_2 Catalysts for the Water-Gas Shift Reaction. *Catalysts* **2017**, *7* (2). https://doi.org/10.3390/catal7020048.

(30) Chen, Y.; Lin, J.; Wang, X. Noble-Metal Based Single-Atom Catalysts for the Water-Gas Shift Reaction. *Chem. Commun.* **2022**, *58* (2), 208–222. https://doi.org/10.1039/D1CC04051K.

(31) Chen, W.-H.; Chen, C.-Y. Water Gas Shift Reaction for Hydrogen Production and Carbon Dioxide Capture: A Review. *Appl. Energy* **2020**, *258* (October), 114078. https://doi.org/10.1016/j.apenergy.2019.114078.

(32) Ning, J.; Zhou, Y.; Shen, W. Atomically Dispersed Copper Species on Ceria for the Low-Temperature Water-Gas Shift Reaction. *Sci. China Chem.* **2021**, *64* (7), 1103–1110. https://doi.org/10.1007/s11426-020-9867-x.

(33) Lykaki, M.; Stefa, S.; Carabineiro, S.; Soria, M.; Madeira, L.; Konsolakis, M. Shape

Effects of Ceria Nanoparticles on the Water–Gas Shift Performance of CuO_x/CeO_2 Catalysts. *Catalysts* **2021**, *11* (6), 753. https://doi.org/10.3390/catal11060753.

(34) Zhou, Y.; Chen, A.; Ning, J.; Shen, W. Electronic and Geometric Structure of the Copper-Ceria Interface on Cu/CeO_2 Catalysts. *Chinese J. Catal.* **2020**, *41* (6), 928–937. https://doi.org/10.1016/S1872-2067(20)63540-9.

(35) Ning, J.; Zhou, Y.; Chen, A.; Li, Y.; Miao, S.; Shen, W. Dispersion of Copper on Ceria for the Low-Temperature Water-Gas Shift Reaction. *Catal. Today* **2019**, No. June, 1–8. https://doi.org/10.1016/j.cattod.2019.07.048.

(36) Vovchok, D.; Guild, C. J.; Llorca, J.; Xu, W.; Jafari, T.; Toloueinia, P.; Kriz, D.; Waluyo, I.; Palomino, R. M.; Rodriguez, J. A.; Suib, S. L.; Senanayake, S. D. Cu Supported on Mesoporous Ceria: Water Gas Shift Activity at Low Cu Loadings through Metal–Support Interactions. *Phys. Chem. Chem. Phys.* **2017**, *19* (27), 17708–17717. https://doi.org/10.1039/C7CP02378B.

(37) Ahn, S. Y.; Na, H. S.; Jeon, K. W.; Lee, Y. L.; Kim, K. J.; Shim, J. O.; Roh, H. S. Effect of Cu/CeO_2 Catalyst Preparation Methods on Their Characteristics for Low Temperature Water−gas Shift Reaction: A Detailed Study. *Catal. Today* **2020**, *352* (June), 166–174. https://doi.org/10.1016/j.cattod.2019.11.017.

(38) Tsoncheva, T.; Mileva, A.; Issa, G.; Henych, J.; Tolasz, J.; Dimitrov, M.; Kovacheva, D.; Atanasova, G.; Štengl, V. Mesoporous Copper-Ceria-Titania Ternary Oxides as Catalysts for Environmental Protection: Impact of Ce/Ti Ratio and Preparation Procedure. *Appl. Catal. A Gen.* **2020**, *595* (February), 117487. https://doi.org/10.1016/j.apcata.2020.117487.

(39) Ziemba, M.; Ganduglia-Pirovano, M. V.; Hess, C. Insight into the Mechanism of the Water–Gas Shift Reaction over Au/CeO_2 Catalysts Using Combined Operando Spectroscopies. *Faraday Discuss.* **2021**, *229*, 232–250. https://doi.org/10.1039/C9FD00133F.

(40) Ziemba, M.; Schilling, C.; Ganduglia-Pirovano, M. V.; Hess, C. Toward an Atomic-Level Understanding of Ceria-Based Catalysts: When Experiment and Theory Go Hand in Hand. *Acc. Chem. Res.* **2021**, *54* (13), 2884–2893. https://doi.org/10.1021/acs.accounts.1c00226.

(41) Konsolakis, M. The Role of Copper–Ceria Interactions in Catalysis Science: Recent Theoretical and Experimental Advances. *Appl. Catal. B Environ.* **2016**, *198*, 49–66. https://doi.org/10.1016/j.apcatb.2016.05.037.

(42) Kang, L.; Wang, B.; Güntner, A. T.; Xu, S.; Wan, X.; Liu, Y.; Marlow, S.; Ren, Y.;

Gianolio, D.; Tang, C. C.; Murzin, V.; Asakura, H.; He, Q.; Guan, S.; Velasco-Vélez, J. J.; Pratsinis, S. E.; Guo, Y.; Wang, F. R. The Electrophilicity of Surface Carbon Species in the Redox Reactions of CuO-CeO_2 Catalysts. *Angew. Chemie* **2021**, *133* (26), 14541–14549. https://doi.org/10.1002/ange.202102570.

(43) Kang, L.; Wang, B.; Bing, Q.; Zalibera, M.; Büchel, R.; Xu, R.; Wang, Q.; Liu, Y.; Gianolio, D.; Tang, C. C.; Gibson, E. K.; Danaie, M.; Allen, C.; Wu, K.; Marlow, S.; Sun, L.; He, Q.; Guan, S.; Savitsky, A.; Velasco-Vélez, J. J.; Callison, J.; Kay, C. W. M.; Pratsinis, S. E.; Lubitz, W.; Liu, J.; Wang, F. R. Adsorption and Activation of Molecular Oxygen over Atomic Copper(I/II) Site on Ceria. *Nat. Commun.* **2020**, *11* (1), 4008. https://doi.org/10.1038/s41467-020-17852-8.

(44) Chen, A.; Yu, X.; Zhou, Y.; Miao, S.; Li, Y.; Kuld, S.; Sehested, J.; Liu, J.; Aoki, T.; Hong, S.; Camellone, M. F.; Fabris, S.; Ning, J.; Jin, C.; Yang, C.; Nefedov, A.; Wöll, C.; Wang, Y.; Shen, W. Structure of the Catalytically Active Copper–Ceria Interfacial Perimeter. *Nat. Catal.* **2019**, *2* (4), 334–341. https://doi.org/10.1038/s41929-019-0226-6.

(45) Yu, W.-Z.; Wu, M.-Y.; Wang, W.-W.; Jia, C.-J. In Situ Generation of the Surface Oxygen Vacancies in a Copper–Ceria Catalyst for the Water–Gas Shift Reaction. *Langmuir* **2021**, *37* (35), 10499–10509. https://doi.org/10.1021/acs.langmuir.1c01428.

(46) Ren, Z.; Liu, N.; Chen, B.; Li, J.; Mei, D. Nucleation of Cu_n (n = 1–5) Clusters and Equilibrium Morphology of Cu Particles Supported on CeO_2 Surface: A Density Functional Theory Study. *J. Phys. Chem. C* **2018**, *122* (48), 27402–27411. https://doi.org/10.1021/acs.jpcc.8b07993.

(47) Yao, S. Y.; Xu, W. Q.; Johnston-Peck, A. C.; Zhao, F. Z.; Liu, Z. Y.; Luo, S.; Senanayake, S. D.; Martínez-Arias, A.; Liu, W. J.; Rodriguez, J. A. Morphological Effects of the Nanostructured Ceria Support on the Activity and Stability of CuO/CeO_2 Catalysts for the Water-Gas Shift Reaction. *Phys. Chem. Chem. Phys.* **2014**, *16* (32), 17183–17195. https://doi.org/10.1039/c4cp02276a.

(48) Müller, P.; Hermans, I. Applications of Modulation Excitation Spectroscopy in Heterogeneous Catalysis. *Ind. Eng. Chem. Res.* **2017**, *56* (5), 1123–1136. https://doi.org/10.1021/acs.iecr.6b04855.

(49) Filtschew, A.; Hofmann, K.; Hess, C. Ceria and Its Defect Structure: New Insights from a Combined Spectroscopic Approach. *J. Phys. Chem. C* **2016**, *120* (12), 6694–6703. https://doi.org/10.1021/acs.jpcc.6b00959.

(50) Ziemba, M.; Weyel, J.; Hess, C. Elucidating the Mechanism of the Reverse Water–Gas

Shift Reaction over Au/CeO_2 Catalysts Using Operando and Transient Spectroscopies. *Appl. Catal. B Environ.* **2022**, *301* (October 2021), 120825. https://doi.org/10.1016/j.apcatb.2021.120825.

(51) Ziemba, M.; Hess, C. Influence of Gold on the Reactivity Behaviour of Ceria Nanorods in CO Oxidation: Combining Operando Spectroscopies and DFT Calculations. *Catal. Sci. Technol.* **2020**, *10* (11), 3720–3730. https://doi.org/10.1039/D0CY00392A.

(52) Nottbohm, C. T.; Hess, C. Investigation of Ceria by Combined Raman, UV–Vis and X-Ray Photoelectron Spectroscopy. *Catal. Commun.* **2012**, *22*, 39–42. https://doi.org/10.1016/j.catcom.2012.02.009.

(53) Schilling, C.; Hess, C. Real-Time Observation of the Defect Dynamics in Working Au/CeO $_2$ Catalysts by Combined Operando Raman/UV–Vis Spectroscopy. *J. Phys. Chem. C* **2018**, *122* (5), 2909–2917. https://doi.org/10.1021/acs.jpcc.8b00027.

(54) Ziemba, M.; Schumacher, L.; Hess, C. Reduction Behavior of Cubic In_2O_3 Nanoparticles by Combined Multiple In Situ Spectroscopy and DFT. *J. Phys. Chem. Lett.* **2021**, *12* (15), 3749–3754. https://doi.org/10.1021/acs.jpclett.1c00892.

(55) Schilling, C.; Ziemba, M.; Hess, C.; Ganduglia-Pirovano, M. V. Identification of Single-Atom Active Sites in CO Oxidation over Oxide-Supported Au Catalysts. *J. Catal.* **2020**, *383*, 264–272. https://doi.org/10.1016/j.jcat.2020.01.022.

(56) Schilling, C.; Hess, C. CO Oxidation on Ceria Supported Gold Catalysts Studied by Combined Operando Raman/UV–Vis and IR Spectroscopy. *Top. Catal.* **2017**, *60* (1–2), 131–140. https://doi.org/10.1007/s11244-016-0732-6.

(57) Weyel, J.; Ziemba, M.; Hess, C. Elucidating Active CO–Au Species on Au/CeO_2(111): A Combined Modulation Excitation DRIFTS and Density Functional Theory Study. *Top. Catal.* **2022**. https://doi.org/10.1007/s11244-022-01599-1.

(58) Li, A.; Yao, D.; Yang, Y.; Yang, W.; Li, Z.; Lv, J.; Huang, S.; Wang, Y.; Ma, X. Active Cu^0 –$Cu^{\sigma+}$ Sites for the Hydrogenation of Carbon–Oxygen Bonds over Cu/CeO_2 Catalysts. *ACS Catal.* **2022**, *12* (2), 1315–1325. https://doi.org/10.1021/acscatal.1c04504.

(59) Ziemba, M.; Stark, D.; Hess, C. Combined DFT and Operando Spectroscopic Study of the Water-Gas Shift Reaction over Ceria Based Catalysts: The Role of the Noble Metal and Ceria Faceting. In *Proceedings of 1st International Electronic Conference on Catalysis Sciences*; MDPI: Basel, Switzerland, 2020; Vol. 2, p 7531. https://doi.org/10.3390/ECCS2020-07531.

(60) Briggs, D.; Seah, M. P. *Practical Surface Analysis by Auger and X-Ray Photoelectron*

Spectroscopy; Wiley, 1983.

(61) Monte, M.; Munuera, G.; Costa, D.; Conesa, J. C.; Martínez-Arias, A. Near-Ambient XPS Characterization of Interfacial Copper Species in Ceria-Supported Copper Catalysts. *Phys. Chem. Chem. Phys.* **2015**, *17* (44), 29995–30004. https://doi.org/10.1039/C5CP04354A.

(62) Szabová, L.; Skála, T.; Matolínová, I.; Fabris, S.; Farnesi Camellone, M.; Matolín, V. Copper-Ceria Interaction: A Combined Photoemission and DFT Study. *Appl. Surf. Sci.* **2013**, *267*, 12–16. https://doi.org/10.1016/j.apsusc.2012.04.098.

(63) Castleton, C. W. M.; Kullgren, J.; Hermansson, K. Tuning LDA+U for Electron Localization and Structure at Oxygen Vacancies in Ceria. *J. Chem. Phys.* **2007**, *127* (24), 244704. https://doi.org/10.1063/1.2800015.

(64) Zabilskiy, M.; Djinović, P.; Tchernychova, E.; Tkachenko, O. P.; Kustov, L. M.; Pintar, A. Nanoshaped CuO/CeO_2 Materials: Effect of the Exposed Ceria Surfaces on Catalytic Activity in N_2O Decomposition Reaction. *ACS Catal.* **2015**, *5* (9), 5357–5365. https://doi.org/10.1021/acscatal.5b01044.

(65) Praliaud, H. Surface and Bulk Properties of Cu–ZSM-5 and Cu/Al_2O_3 Solids during Redox Treatments. Correlation with the Selective Reduction of Nitric Oxide by Hydrocarbons. *Appl. Catal. B Environ.* **1998**, *16* (4), 359–374. https://doi.org/10.1016/S0926-3373(97)00093-3.

(66) Pestryakov, A. N.; Petranovskii, V. P.; Kryazhov, A.; Ozhereliev, O.; Pfänder, N.; Knop-Gericke, A. Study of Copper Nanoparticles Formation on Supports of Different Nature by UV–Vis Diffuse Reflectance Spectroscopy. *Chem. Phys. Lett.* **2004**, *385* (3–4), 173–176. https://doi.org/10.1016/j.cplett.2003.12.077.

(67) Chan, G. H.; Zhao, J.; Hicks, E. M.; Schatz, G. C.; Van Duyne, R. P. Plasmonic Properties of Copper Nanoparticles Fabricated by Nanosphere Lithography. *Nano Lett.* **2007**, *7* (7), 1947–1952. https://doi.org/10.1021/nl070648a.

(68) Bu, Y.; Niemantsverdriet, J. W. H.; Fredriksson, H. O. A. Cu Model Catalyst Dynamics and CO Oxidation Kinetics Studied by Simultaneous in Situ UV–Vis and Mass Spectroscopy. *ACS Catal.* **2016**, *6* (5), 2867–2876. https://doi.org/10.1021/acscatal.5b02861.

(69) Romero-Sarria, F.; Martínez T, L. M.; Centeno, M. A.; Odriozola, J. A. Surface Dynamics of Au/CeO_2 Catalysts during CO Oxidation. *J. Phys. Chem. C* **2007**, *111* (39), 14469–14475. https://doi.org/10.1021/jp073541k.

(70) Vayssilov, G. N.; Mihaylov, M.; Petkov, P. S.; Hadjiivanov, K. I.; Neyman, K. M.

Reassignment of the Vibrational Spectra of Carbonates, Formates, and Related Surface Species on Ceria: A Combined Density Functional and Infrared Spectroscopy Investigation. *J. Phys. Chem. C* **2011**, *115* (47), 23435–23454. https://doi.org/10.1021/jp208050a.

(71) Yang, S.-C.; Pang, S. H.; Sulmonetti, T. P.; Su, W.-N.; Lee, J.-F.; Hwang, B.-J.; Jones, C. W. Synergy between Ceria Oxygen Vacancies and Cu Nanoparticles Facilitates the Catalytic Conversion of CO_2 to CO under Mild Conditions. *ACS Catal.* **2018**, *8* (12), 12056–12066. https://doi.org/10.1021/acscatal.8b04219.

(72) Daly, H.; Ni, J.; Thompsett, D.; Meunier, F. C. On the Usefulness of Carbon Isotopic Exchange for the Operando Analysis of Metal-Carbonyl Bands by IR over Ceria-Containing Catalysts. *J. Catal.* **2008**, *254* (2), 238–243. https://doi.org/10.1016/j.jcat.2007.12.013.

(73) Isokoski, K.; Poteet, C. A.; Linnartz, H. Highly Resolved Infrared Spectra of Pure CO_2 Ice (15–75 K). *Astron. Astrophys.* **2013**, *555*, A85. https://doi.org/10.1051/0004-6361/201321517.

(74) Laachir, A.; Perrichon, V.; Badri, A.; Lamotte, J.; Catherine, E.; Lavalley, J. C.; El Fallah, J.; Hilaire, L.; Le Normand, F.; Quéméré, E.; Sauvion, G. N.; Touret, O. Reduction of CeO_2 by Hydrogen. Magnetic Susceptibility and Fourier-Transform Infrared, Ultraviolet and X-Ray Photoelectron Spectroscopy Measurements. *J. Chem. Soc. Faraday Trans.* **1991**, *87* (10), 1601–1609. https://doi.org/10.1039/FT9918701601.

(75) Badri, A.; Binet, C.; Lavalley, J. An FTIR Study of Surface Ceria Hydroxy Groups during a Redox Process with H_2. *J. Chem. Soc. Faraday Trans.* **1996**, *92* (23), 4669. https://doi.org/10.1039/ft9969204669.

(76) Bera, P.; Cámara, A. L.; Hornés, A.; Martínez-Arias, A. Comparative in Situ DRIFTS-MS Study of ^{12}CO- and ^{13}CO-TPR on CuO/CeO_2 Catalyst. *J. Phys. Chem. C* **2009**, *113* (24), 10689–10695. https://doi.org/10.1021/jp9020504.

(77) Gao, X.; Lin, X.; Xie, X.; Li, J.; Wu, X.; Li, Y.; Kawi, S. Modification Strategies of Heterogeneous Catalysts for Water–Gas Shift Reactions. *React. Chem. Eng.* **2022**, *7* (3), 551–565. https://doi.org/10.1039/D1RE00537E.

(78) Salcedo, A.; Irigoyen, B. Unraveling the Origin of Ceria Activity in Water–Gas Shift by First-Principles Microkinetic Modeling. *J. Phys. Chem. C* **2020**, *124* (14), 7823–7834. https://doi.org/10.1021/acs.jpcc.0c00229.

(79) Wu, Z.; Li, M.; Overbury, S. H. On the Structure Dependence of CO Oxidation over

CeO_2 Nanocrystals with Well-Defined Surface Planes. *J. Catal.* **2012**, *285* (1), 61–73. https://doi.org/10.1016/j.jcat.2011.09.011.